2013

Excited State Calculations In Solids By Auxiliary-Field Quantum Monte Carlo

Fengjie Ma
William and Mary

Shiwei Zhang

Henry Krakauer
William & Mary

Recommended Citation

Ma, F., Zhang, S., & Krakauer, H. (2013). Excited state calculations in solids by auxiliary-field quantum Monte Carlo. New Journal of Physics, 15(9), 093017.

New Journal of Physics
The open access journal at the forefront of physics

Deutsche Physikalische Gesellschaft DPG IOP Institute of Physics

PAPER • OPEN ACCESS

Excited state calculations in solids by auxiliary-field quantum Monte Carlo

To cite this article: Fengjie Ma *et al* 2013 *New J. Phys.* **15** 093017

New Journal of Physics
The open access journal for physics

Excited state calculations in solids by auxiliary-field quantum Monte Carlo

Fengjie Ma, Shiwei Zhang and Henry Krakauer
Department of Physics, College of William and Mary, Williamsburg, VA 23187, USA
E-mail: fma01@wm.edu, shiwei@wm.edu and hxkrak@wm.edu

New Journal of Physics **15** (2013) 093017 (11pp)
Received 11 April 2013
Published 13 September 2013
Online at http://www.njp.org/
doi:10.1088/1367-2630/15/9/093017

Abstract. We present an approach for *ab initio* many-body calculations of excited states in solids. Using auxiliary-field quantum Monte Carlo, we introduce an orthogonalization constraint with virtual orbitals to prevent collapse of the stochastic Slater determinants in the imaginary-time propagation. Trial wave functions from density-functional calculations are used for the constraints. Detailed band structures can be calculated. Results for standard semiconductors are in good agreement with experiments; comparisons are also made with GW calculations and the connections and differences are discussed. For the challenging ZnO wurtzite structure, we obtain a fundamental band gap of 3.26(16) eV, consistent with experiments.

Contents

1. Introduction

The accurate calculation of excited states in extended systems is a leading challenge in modern electronic structure theory. Density functional theory (DFT), which usually gives good results for ground state properties of materials without strong electron correlation, suffers from the well-known band-gap problem even for simple semiconductors [1–3]. The use of hybrid functionals, which incorporate a portion of exact exchange from Hartree–Fock (HF) theory, has resulted in significant improvements for semiconductors with small to medium gaps, but less so for large gap systems [4]. Time-dependent DFT and many-body perturbative approaches have shown considerable promise [5]. The *GW* method is perhaps the simplest and most widely used of the latter and has led to dramatically improved results, largely for simple sp bonded materials [6]. It is less successful in materials that are more strongly correlated. In wurtzite structure ZnO, for example, the accuracy of *GW* quasi-particle excitation energies is still a matter of some controversy [7–11]. A general approach which allows accurate calculations of electronic excitations across a wide variety of solids is thus very much in need.

Quantum Monte Carlo (QMC) [12, 13] is a non-perturbative, many-body computational method which is uniquely capable of scaling up to large system sizes and which in principle does not involve empirical parameters. Ground-state calculations with several flavors of QMC have seen significant recent development [12–14]. Although some excited states calculations have also been performed, for example, calculations in molecules [15, 16] and diffusion Monte Carlo (DMC) calculations of excitation energies of silicon and diamond at some high symmetry k-points [17, 18], the capability of QMC to treat excited states in general is much less developed. A major reason for this is the intrinsic difficulty of maintaining orthogonality with the lower-lying states when the targeted many-body excited state is being represented stochastically in an imaginary-time projection method.

The auxiliary-field quantum Monte Carlo (AFQMC) method ([13] and references therein) naturally offers a new framework for addressing this difficulty and for doing excited state calculations in solids. The random walks in AFQMC take place in a space of Slater determinants. The single-particle orbitals in each Slater determinant are expressed explicitly in terms of a chosen one-particle basis. Thus, in addition to orthogonalizing the single-particle

orbitals with each other (as is done in ground-state calculations), one can orthogonalize them with empty (hole) orbitals to remove contamination in the projection. For example, as an approximate constraint, the occupied orbitals can be orthogonalized with unoccupied ones defined by a trial wave function. Recent developments in ground state calculations have demonstrated that the AFQMC framework, with properly formulated sign or phase constraints using trial wave functions, allows sign-problem-free simulations with high accuracy across a wide range of both strongly correlated model Hamiltonians [19] and real material systems [13, 20–25].

In this paper, we show how the AFQMC approach can be formulated to accurately calculate excited states in extended systems. The ground-state method is augmented by an orthogonalization constraint with virtual orbitals to prevent collapse to lower-lying states in the imaginary-time projection. Simple trial wave functions from HF or DFT are used for the phaseless and orthogonalization constraints. We illustrate the method by calculating the detailed band structures in silicon and carbon, which are, respectively, small and large band gap semiconductors. We then apply the method to determine the optical band gap in ZnO, which has drawn much recent attention and which presents a significant challenge, with high-lying strongly correlated 3d-bands interacting with 3s and 3p semicore states.

2. Methodology

2.1. Formalism

We focus on optical gaps, from the creation of a bounded electron–hole (eh) pair (exciton) with infinite lifetime. In AFQMC, we target an excited state of the many-body Hamiltonian $\hat{H}$ with imaginary-time projection $|\Psi^*(\beta)\rangle \propto \mathrm{e}^{-\beta\hat{H}}|\psi_{\mathrm{T}}^*\rangle$, where $|\psi_{\mathrm{T}}^*\rangle$ is a trial wave function of the excited state, and $\beta \equiv N\Delta\tau$ with N the simulation time step and $\Delta\tau$ the Trotter step size. The wave function at any imaginary-time can be thought of as $|\Psi^*(\beta)\rangle = \sum_\phi c_\phi\, |\phi_\uparrow\rangle \otimes |\phi_\downarrow\rangle$. Each Slater determinant in the sum, $|\phi_\uparrow\rangle \otimes |\phi_\downarrow\rangle$, is a random walker whose orbitals (mutually orthogonal initially) evolve with imaginary-time β. The distribution of the random walkers gives a statistical representation of the coefficients c_ϕ. Explicitly, $|\phi_\uparrow\rangle$ has the form $(\phi_1, \ldots, \phi_i, \ldots, \phi_m)$, where each ϕ_i is an orbital that evolves with β, and m denotes the number of spin-$\uparrow$ electrons. (Below we will suppress the spin index where possible; the $\downarrow$ component has a similar form.) Thus the AFQMC process resembles the propagation of a population of mean-field solutions in time-dependent external fields. As the orbitals evolve during the random walk, some non-orthogonality will develop. As long as the orbitals remain linearly independent, the walker determinant is independent of this. Eventually, however, the tendency to collapse to an unphysical bosonic ground state would create numerical instabilities due to finite arithmetic precision. To prevent this, periodically in the propagation the orbitals within each random walker are orthogonalized with each other to ensure that the signal for fermionic antisymmetry is not lost in numerical noise. This step is also needed in ground-state calculations [26], and indeed even in mean-field calculations. Note that, although the orbitals in each random walker at any given time β can be thought of as being orthogonal, different random walkers, or the same walker at different times, are in general not orthogonal to each other in AFQMC.

The excited state energy can be calculated by the mixed estimator [16]

$$E^*(\beta) = \frac{\langle\psi_{\mathrm{T}}^*|\hat{H}|\Psi^*(\beta)\rangle}{\langle\psi_{\mathrm{T}}^*|\Psi^*(\beta)\rangle}, \tag{1}$$

which converges to the exact result at $\beta \to \infty$. If $|\psi_T^*\rangle$ belongs to an irreducible representation of the symmetry group of $\hat{H}$ different from that of the ground state, equation (1) is exact for the lowest excited state of that symmetry. Otherwise, imaginary-time projection is considerably more challenging, since the propagation will tend to collapse to the ground state (or other lower-lying states) [16].

The AFQMC formalism, however, provides a natural way to prevent the collapse. The orbital structure of the random walker in AFQMC allows one to impose additional orthogonality constraints, using virtual orbitals. For a concrete illustration, consider a targeted many-body state corresponding to the 'single' excitation of replacing the ith valence orbital by conduction orbital labeled by j (thus $j > m$). Each random walker is still an m-electron Slater determinant. For the purpose of orthogonalization, however, we will regard it as the extended ordered list $(\phi_1, \ldots, \phi_{i-1}, \bar{\phi}_i, \phi_{i+1}, \ldots, \phi_m, \bar{\phi}_{m+1}, \ldots, \bar{\phi}_{j-1}, \phi_j)$. Any orbital denoted by '-' is a virtual orbital whose *only* role is in the orthogonalization of the m occupied orbitals. A Gram–Schmidt orthogonalization on this extended set ensures the following orthogonality conditions:

(i) $\langle \bar{\phi}_i | \phi_j \rangle = 0$;
(ii) $\langle \bar{\phi}_i | \phi_k \rangle = 0$ for $k \in [i+1, m]$;
(iii) $\langle \bar{\phi}_k | \phi_j \rangle = 0$ for $k \in [m+1, j-1]$.

After the orthogonalization step, only the m occupied orbitals are retained and included in the propagation and measurement, until the next time for orthogonalization when the $\bar{\phi}$ are re-inserted and the procedure repeated. This extended Gram–Schmidt procedure adds minimally to the total CPU time, which is dominated by the projection and local-energy evaluations. (Timing information on the plane-wave AFQMC formalism, which is used in this work, has been discussed in [20–22].) The procedure generalizes straightforwardly if the targeted excited state corresponds to 'double' excitations or beyond.

In the present study, we use the corresponding orbitals from mean-field theory as the virtual orbitals in the orthogonalization, as discussed below. The orthogonality constraint is *exact* within independent-particle theory, and a natural generalization in the spirit of the phaseless approximation [13] when the auxiliary-fields are activated. It stabilizes calculations of an excited state, even if the latter is not the lowest energy state of that symmetry.

We take simple trial wave functions directly from DFT calculations for the phaseless constraint [13] and for the orthogonalization. The starting point for constructing $|\psi_T^*(k)\rangle$ at the selected k point in the Brillouin zone (BZ) is the single Slater determinant DFT wave function for the ground state, $|\psi_T(k)\rangle$. The orbitals $\phi_{\sigma,i}^T$ are given by the eigenfunctions at k based on a well-converged density integrated over k-points. For a given excitation of spin-σ from an occupied orbital i to an unoccupied orbital j, we replace $\phi_{i,\sigma}^T$ by $\phi_{j,\sigma}^T$. In the orthogonality constraint, we use the corresponding DFT orbitals, i.e. $\bar{\phi}_i = \phi_i^T$. Virtual orbitals derived from different DFT calculations (local density approximation (LDA), generalized gradient approximation (GGA) and hybrids) give essentially the same results. The insensitivity of AFQMC to the choice of trial wave function has been previously noted [20, 23].

For insulators, the ground states are closed shell configurations, so this type of excited state Slater determinant will be spin-contaminated in general. To avoid this, we form a two-determinant singlet wave function

$$|\psi_T^*\rangle = (a_{j\uparrow}^\dagger a_{i\uparrow} + a_{j\downarrow}^\dagger a_{i\downarrow})|\psi_T\rangle, \tag{2}$$

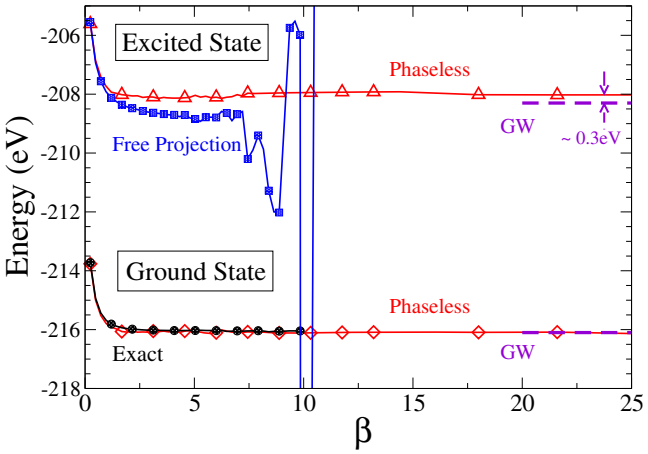

Figure 1. Illustration of AFQMC projections of the ground- and excited-state ($i = 2 \rightarrow j = 5$) energies (equation (1)) in silicon at $k = (0.3, 0, 0)$. Phaseless AFQMC result for the ground state (red diamonds) is compared to exact free-projection (black circles). For the excited state, free-projection (blue squares) collapses. Result from the new method with phaseless and virtual orthogonalization constraint is shown in red triangles. *GW* excitation is shown for reference and is indicated by violet dashed lines [27].

where $a_j^\dagger$ and a_i are creation and destruction operators for unoccupied (conduction) and occupied (valence) states, respectively, and we assume that the spatial part of the valence and conduction orbitals are spin independent. In degenerate cases, the trial wave function is constructed by considering all possible promotions among these orbitals, and the coefficients of each determinant are set equal. In the orthogonality constraint, if the valence state ϕ_i^{T} is degenerate, its partners are not included in the constraint, which is consistent with ground state AFQMC for an open-shell system. Similarly, any degenerate partners of the conduction state ϕ_j^{T} are not included. All our calculations are performed at arbitrary k-points in the primitive cell that holds the most complete symmetry for different excitations. In supercells, the folding of bands creates additional mixing of crystal momentum eigenstates, whose decoupling at the many-body level will need further study.

2.2. *Illustration*

Figure 1 illustrates our method in fcc silicon. The excited state corresponds to the excitation from band $i = 2$ to the lowest lying conduction band $j = 5$ at $k = (0.3, 0, 0)$. The trial wave function $|\psi_{\mathrm{T}}\rangle$ was obtained from DFT with the LDA, while $|\psi_{\mathrm{T}}^*\rangle$ for excited state is the singlet trial wave function of equation (2). For comparison, AFQMC results are also shown from free-projection, which does not impose the phaseless constraint [13] and is exact for the ground state, but is eventually overwhelmed by the fermion sign problem. (Large runs with $\sim 2 \times 10^6$ walkers were used in the free-projection calculations.) The ground state phaseless AFQMC results are in excellent agreement with the exact calculation, indicating very small systematic error from the phaseless approximation, consistent with earlier results [21]. In contrast with the ground state, exactness is not ensured in free projection for the excited state; a more severe sign problem and onset of collapse is seen. The phaseless and the orthogonality constraints stabilize the excited

state calculation and yield an accurate excitation energy, which is within ~ 0.3 eV of the *GW* result [27] after correction of finite-size (FS) effects, as we discuss next.

2.3. Calculation of the band structure and discussion

Excitation energies from valence state i to conduction state j at any selected BZ k point are calculated as the difference between the AFQMC total energy and the corresponding ground-state energy

$$\Delta E_{ij}^{\mathrm{QMC}}(k) = E_{ij}^{*}(k) - E_0(k). \tag{3}$$

Because the many-body calculations are performed in FS simulation cells, the energies have FS errors which must be removed [24, 28–31]. FS corrections to the thermodynamic limit can be obtained as post-processing corrections [24, 30] from lower-levels of theory for both one-body (1b) and two-body (2b) effects. In excited state calculations, the creation of the eh pair results in an additional bias, from the interaction between the particle and hole. We obtain the combined 1b and eh FS correction from DFT calculations:

$$\delta E_{ij}^{\mathrm{eh,1b}}(k) = e_g(k) - \Delta E_{ij}^{\mathrm{DFT}}(k)\,, \tag{4}$$

where $e_g(k) \equiv e_j(k) - e_i(k)$ is the difference in band energies from a standard DFT calculation, using a dense k-point grid, while $\Delta E_{ij}^{\mathrm{DFT}}(k)$ is from self-consistent DFT calculations at k paralleling the QMC calculations in equation (3). We correct the 2b FS error, which along with the 1b effect are substantially reduced here because $\Delta E_{ij}^{\mathrm{QMC}}(k)$ is an energy difference between two states within the same simulation cell, using

$$\delta E_{ij}^{\mathrm{2b}}(k) = \Delta E_{ij}^{\mathrm{LDA}}(k) - \Delta E_{ij}^{\mathrm{FS-LDA}}(k)\,, \tag{5}$$

where the two excitation energies on the right are from LDA calculations paralleling the QMC, using the standard and a specially parametrized FS functional [24, 30], respectively. The sum of equations (4) and (5) gives the total FS correction $\delta E_{ij}(k)$. The largest contribution is from $\delta E_{ij}^{\mathrm{eh,1b}}(k)$, typically ~ 0.10 eV in the primitive unit cell of Si and diamond. Its largest value in Si is 0.35 eV at the Γ point. In diamond, which has a large band gap, its largest value is 0.83 eV. The 2b correction is typically smaller; its largest value is 0.12 eV in Si and diamond, and 0.08 eV for the fundamental gap in ZnO.

We then obtain a quasiparticle band structure $\epsilon_n(k)$ from a least-squares fit [17] to the calculated many-body excitation energies $\Delta E_{ij}(k) \equiv \Delta E_{ij}^{\mathrm{QMC}}(k) + \delta E_{ij}(k)$:

$$\min\left(\sum_{i\in v}\sum_{j\in c}\left(\Delta E_{ij}(k) - [\epsilon_j(k) - \epsilon_i(k)]\right)^2\right), \tag{6}$$

where i and j run over the occupied (v) and unoccupied (c) states, respectively. There could be a constant energy shift (universal to all bands) between different k-points. For comparison, the highest occupied quasiparticle energy is set equal to the corresponding DFT eigenvalue: $\epsilon_m(k) = e_m(k)$.

As mentioned, the aim of the present QMC calculations is optical gaps. In a large variety of systems, the AFQMC method has shown to be a highly accurate, parameter-free post-DFT method in ground-state calculations using the phaseless constraint with single-determinant trial wave functions from DFT. The present 'promotion' approach addresses the problem in the spirit of capturing excitations described by number conserving eh pair excited states corresponding to

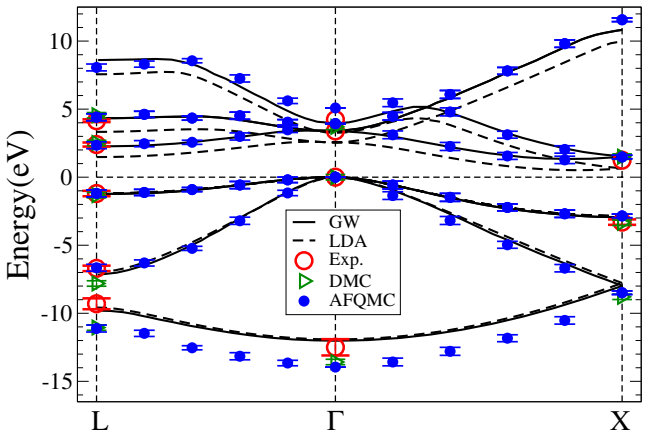

Figure 2. Many-body band structure of silicon from AFQMC (blue dots). *GW* [27] and LDA band structures are plotted by solid and dashed lines, respectively. Available DMC results at high symmetry points Γ, *X* and *L* [17] are indicated by green triangle. Experimental values [27] are shown as red circles.

poles in the Lehman representation of the linear density response function [32]. The orbital orthogonality approximation we have used in the present study assumes that the ordering of many-body excited states produced by the single-determinant trial state in a Koopman's sense is not fundamentally wrong. We will make comparisons with *GW* in discussing our results. However, it is important to note that *GW* calculates addition/removal energies and corresponding gaps. In principle, these are larger than the optical band gap by the exciton binding energy, which is small for all the systems studied here. For Si, the exciton binding energy is about 0.015 eV [33].

We could, of course, also use AFQMC to directly calculate the addition/removal electron excitation energy. There are advantages and disadvantages versus the 'promotion' approach. For the fundamental gap, for example, the addition/removal approach will involve three ground-state total energy calculations [$E(N+1)$, $E(N)$, $E(N-1)$], so it will not have the limitation above of the assumption about the excited state ordering as given by a single Slater determinant trial wave function. On the other hand, FS extrapolation will be much more challenging for the charged systems. The 'promotion' approach within the assumptions above applies to all k-points and can be used to obtain the entire band structure. We will focus on the application of the latter approach in the rest of this paper.

3. Applications

3.1. The band structure of silicon

The calculated full many-body silicon band structure is shown in figure 2 and compared to LDA and *GW*, as well as to available DMC and experimental results [17, 27]. As discussed above, because of small excitonic effect, *GW*'s addition/removal band structure is used as reference. Calculations for fcc silicon were done at the experimental lattice constant of 5.431 Å. Both AFQMC and DFT calculations used a norm-conserving separable nonlocal LDA pseudopotentials generated by the OPIUM code [34], with a planewave cutoff $E_{\rm cut} = 25$ Ryd.

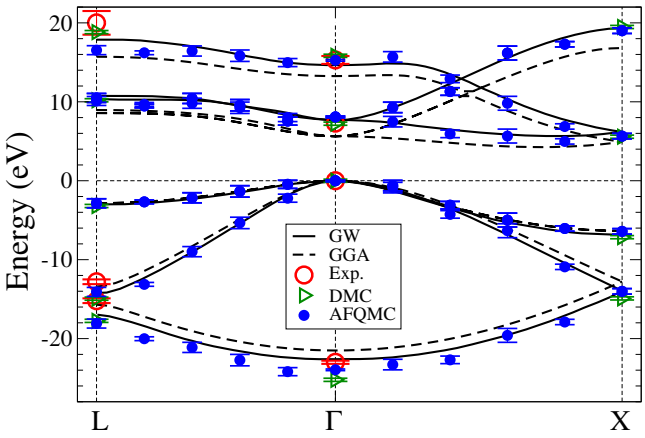

Figure 3. Many-body band structure of diamond from AFQMC (blue dots). *GW* [35] and GGA band structures are plotted by solid and dashed lines, respectively. Available DMC results at high symmetry points Γ, *X* and *L* [18] are indicated by green triangles. Experimental values [27] are shown as red circles.

FS correction has been applied to the AFQMC results to remove residual FS effects, which are small, as discussed in section 2.3. Trotter time-step extrapolation of calculated band gaps in standard semiconductors such as silicon and diamond (as discussed below) shows that Trotter errors are less than the statistical uncertainty (0.02 eV) for $\Delta\tau = 0.005\,\mathrm{Ryd}^{-1}$. Using a $|\psi_T^*\rangle$ from LDA, AFQMC results correct the band gap problem and are in good agreement with experiment and with *GW*. The lowest band, which corresponds to the highest excitation energies, tends to be too low. For an imaginary-time projection method, its quality can be expected to decline for higher excited states. Also the simple singlet $|\psi_T^*\rangle$ or the orthogonalization constraint may not be sufficient, as there are many states with similar energies.

3.2. The band structure of diamond

The many-body band structure of diamond is given in figure 3 together with available DMC and experimental results [18, 27]. The lattice constant of 3.567 Å was used. The calculations are similar to those in Si, except for a higher planewave cutoff $E_{\mathrm{cut}} = 50\,\mathrm{Ryd}$ and the use of GGA pseudopotential and trial wave function. We have verified that the calculations are insensitive to the difference in $|\psi_T^*\rangle$ at the level of LDA versus GGA or a hybrid functional. Other calculational details are similar to those in section 3.1. Exciton binding energy is about 0.08 eV in diamond [36]. The AFQMC results are again generally in very good agreement with *GW* and with experiment.

3.3. The band gap of ZnO

Accurately calculating the fundamental band gap of wurtzite structure ZnO is very challenging. LDA and GGA underestimate the gap by almost 3 eV. Even the generally more accurate *GW* method gives various values [7–11]. There has been considerable discussion about the importance of various convergence issues, choice of pseudopotentials and additional approximations such as the plasmon-pole model and the inclusion of self-consistency in the *GW* calculation [7–11]. Here we will use the AFQMC method to study the full many-body

Table 1. The calculated AFQMC band gap (eV) of wurtzite ZnO, compared to experiments [37–40]. Also shown are results from GGA, hybrid DFT [41, 42] and *GW* [7, 11]. (Experimental exciton binding energy is ~ 0.06 eV [33].)

	GGA	Hybrid	*GW*	AFQMC	Exp.
Δ_{gap}	0.77	3.32,2.90	3.4,3.6,2.56	3.26(16)	3.30,3.44,3.57

Hamiltonian by using high-quality pseudopotential in an *ab initio* way. The orbital orthogonality constraint is applied to guide the propagation, and its stability has been illustrated before. To properly treat the large spatial overlap among 3s, 3p and 3d wave functions of atomic Zn [9], our Zn GGA pseudopotential was constructed with a Ne-core, thereby fully correlating the semicore 3s, 3p along with the 3d states in the many-body calculation. Very conservative radial cutoffs of 0.83, 1.02 and 1.13 Bohr were used for s, p and d channels, respectively, resulting in a large planewave cutoff $E_{\text{cut}} = 180$ Ryd. The pseudopotential gives GGA optimized lattice parameters of $a = 3.279$ and $c = 5.284$ Å, and bulk modulus of 128.7 GPa, all in good agreement with published GGA results [43].

Our AFQMC calculations were done at the above GGA optimized geometry. While hybrid functionals seem to perform better in ZnO, we chose to use simple trial wave functions from GGA in our AFQMC calculations to avoid any parameter tuning. The singlet form $|\psi_{\text{T}}^{*}\rangle$ in equation (2) was used. The main calculations were done with Trotter time-steps of $\Delta\tau = 0.01$ and $0.005\,\text{Ryd}^{-1}$. The Trotter error was then corrected for by extrapolation from separate runs using a single-determinant $|\psi_{\text{T}}^{*}\rangle$. (The Trotter error at $\Delta\tau = 0.005\,\text{Ryd}^{-1}$ is about $\simeq 0.25$ eV prior to extrapolation.) The calculated raw band gap was 2.54(14) eV. Since DFT severely underestimates the band gap, the FS correction is less straightforward in ZnO. At $k = \Gamma$, for example, the single k-point self-consistent GGA calculation would yield a metallic ground state. We extrapolated $\delta E_{ij}^{\text{eh,1b}}(k)$ for k within 0.1 of the Γ point, along two high symmetry lines. In doing so, we assume that the eh effect does not introduce a discontinuity in the band dispersion, which is reasonable since it mainly relates to the simulation cell size. This yielded $\delta E_{ij}^{\text{1b,eh}}(0) = 0.58(08)$ eV (LDA would yield 0.41(04) eV). The 2b correction of equation (5) is well-behaved: $\delta E_{ij}^{\text{2b}}(0) = 0.08$ eV. Adding the FS corrections yields our calculated band gap of 3.20(16) eV.

The experimental equilibrium geometry is at $a = 3.250$ and $c = 5.207$ Å [44]. To compare our band gap (for the GGA equilibrium geometry) to experiment, we apply a correction of +0.06 eV, which is the excitation energy difference given by GGA for the experimental and GGA-optimized geometries. (Hybrid B3LYP calculations give a correction of +0.10 eV.) Table 1 compares our final calculated band gap with optical experimental values and representative results from recent calculations. The error bar on the AFQMC result reflects the statistical error and the uncertainty in the FS corrections.

We note that, even with the small-core pseudopotential, there can be pseudoization and core-relaxation errors [45]. The precise effect cannot be determined without further many-body calculations. However, recent studies [10, 11] comparing all-electron and pseudopotential *GW* calculations indicate that the effect is approximately +0.27 eV for a pseudopotential of similar quality to the one we have adopted. This would increase the AFQMC result for the fundamental band gap in ZnO to $\sim 3.53(16)$ eV, still within the range of experimental measurements but would seem to be in better agreement with the most recent result of 3.57 eV [39, 40].

4. Discussion and summary

We have generalized a powerful AFQMC approach to excited state calculations, and carried out a first set of applications. There are many directions for future research, and various further improvements can be explored. We have used a planewave basis and norm-conserving pseudopotentials in these calculations. Other single-particle basis sets are straightforward to use, for example, with localized or natural orbitals. The former might be useful in the study of localized (Frenkel) excitons. One could also work with a truncated set of orbitals from a lower-level of theory, or use a down-folded Hamiltonian directly to improve computational efficiency. The constraining virtual orbitals have been fixed in our calculations, but could potentially be allowed to dynamically evolve in some way. It is reassuring that DFT trial wave functions have worked well. The overall constraint can be further improved by using better trial wave functions, as we have illustrated in molecules [16]. More elaborate multi-determinant wave functions can be used, for example, from diagonalization in a subspace formed by single and double excitations to conduction orbitals. Furthermore, it may be possible to use AFQMC results as feedback to improve the orthogonality constraint. For example, natural orbitals obtained from the calculated 1b density matrix might be useful in this regard.

In summary, we have presented an AFQMC approach for the calculation of electronic excitations in solids, introducing an orbitally based orthogonalization constraint in the phaseless AFQMC framework to stabilize the projection of excited states. Simple trial wave functions directly from DFT calculations were used for the constraint. Detailed many-body quasiparticle band structures can be calculated. In prototypical semiconductors (Si and diamond), the calculated band structures are in good agreement with those from *GW* calculations and with experiment. In the more strongly correlated and challenging wurtzite ZnO crystal, the calculated fundamental gap is in excellent agreement with the latest experimental data. The method is non-perturbative and free of empirical parameters, offering a possible path for general computations in correlated materials.

Acknowledgments

This work is supported by DOE (DE-FG02-09ER16046; DE-SC0008627), NSF (DMR-1006217) and ONR (N000140811235; N000141211042). An award of computer time was provided by the Innovative and Novel Computational Impact on Theory and Experiment (INCITE) program, using resources of the Oak Ridge Leadership Computing Facility at the Oak Ridge National Laboratory, which is supported by the Office of Science of the US Department of Energy under contract no. DE-AC05-00OR22725. We also acknowledge the computing support from Blue Water at NCSA and the Center for Piezoelectrics by Design. We thank W Purwanto for many useful discussions, and Eric J Walter for help with pseudopotentials.

References

[1] Hohenberg P and Kohn W 1964 *Phys. Rev.* **136** B864
[2] Kohn W and Sham L J 1965 *Phys. Rev.* **140** A1133
[3] Perdew J P and Levy M 1983 *Phys. Rev. Lett.* **51** 1884
[4] Becke A D 1993 *J. Chem. Phys.* **98** 1372
[5] Onida G, Reining L and Rubio A 2002 *Rev. Mod. Phys.* **74** 601
[6] Hedin L 1965 *Phys. Rev.* **139** A796

[7] Shih B C, Xue Y, Zhang P, Cohen M L and Louie S G 2010 *Phys. Rev. Lett.* **105** 146401
[8] Stankovski M, Antonius G, Waroquiers D, Miglio A, Dixit H, Sankaran K, Giantomassi M, Gonze X, Côté M and Rignanese G M 2011 *Phys. Rev.* B **84** 241201
[9] Partoens H D, Saniz R, Lamoen D and Partoens B 2010 *J. Phys.: Condens Matter* **22** 125505
[10] Friedrich C, Müller M C and Blügel S 2011 *Phys. Rev.* B **83** 081101
Friedrich C, Müller M C and Blügel S 2011 *Phys. Rev.* B **84** 039906
[11] Berger J A, Reining L and Sottile F 2012 *Phys. Rev.* B **85** 085126
[12] Foulkes W M C, Mitas L, Needs R J and Rajagopal G 2001 *Rev. Mod. Phys.* **73** 33
[13] Zhang S and Krakauer H 2003 *Phys. Rev. Lett.* **90** 136401
[14] Booth G H, Thom A J W and Alavi A 2009 *J. Chem. Phys.* **131** 054106
[15] Schautz F, Buda F and Filippi C 2004 *J. Chem. Phys.* **121** 5836
[16] Purwanto W, Zhang S and Krakauer H 2009 *J. Chem. Phys.* **130** 094107
[17] Williamson A, Hood R, Needs R and Rajagopal G 1998 *Phys. Rev.* B **57** 12140
[18] Towler M D, Hood R Q and Needs R J 2000 *Phys. Rev.* B **62** 2330
[19] Chang C C and Zhang S 2008 *Phys. Rev.* B **78** 165101
[20] Suewattana M, Purwanto W, Zhang S, Krakauer H and Walter E J 2007 *Phys. Rev.* B **75** 245123
[21] Purwanto W, Krakauer H and Zhang S 2009 *Phys. Rev.* B **80** 214116
[22] Al-Saidi W A, Krakauer H and Zhang S 2007 *J. Chem. Phys.* **126** 194105
[23] Al-Saidi W A, Zhang S and Krakauer H 2006 *J. Chem. Phys.* **124** 224101
[24] Kwee H, Zhang S and Krakauer H 2008 *Phys. Rev. Lett.* **100** 126404
[25] Al-Saidi W A, Krakauer H and Zhang S 2006 *Phys. Rev.* B **73** 075103
[26] Zhang S, Carlson J and Gubernatis J E 1997 *Phys. Rev.* B **55** 7464
[27] Rohlfing M, Krüger P and Pollmann J 1993 *Phys. Rev.* B **48** 17791
[28] Kent P R C, Hood R Q, Williamson A J, Needs R J, Foulkes W M C and Rajagopal G 1999 *Phys. Rev.* B **59** 1917
[29] Chiesa S, Ceperley D, Martin R and Holzmann M 2006 *Phys. Rev. Lett.* **97** 076404
[30] Ma F, Zhang S and Krakauer H 2011 *Phys. Rev.* B **84** 155130
[31] Drummond N D, Needs R J, Sorouri A and Foulkes W M C 2008 *Phys. Rev.* B **78** 125106
[32] Fetter A L and Walecka J D 1971 *Quantum Theory of Many-Particle Systems* (New York: McGraw-Hill)
[33] Dvorak M, Wei S and Wu Z 2013 *Phys. Rev. Lett.* **110** 016402
[34] Walter E J The Opium project (http://opium.sourceforge.net)
[35] Faleev S V, van Schilfgaarde M, Kotani T, Léonard F and Desjarlais M P 2006 *Phys. Rev.* B **74** 033101
[36] Dean P J, Lightowlers E C and Wight D R 1965 *Phys. Rev.* **140** A352
[37] Srikant V and Clarke D R 1998 *J. Appl. Phys.* **83** 5447
[38] Mang A, Reimann K and Rübenacke S 1995 *Solid State Commun.* **94** 251
[39] Tsoi S, Lu X, Ramdas A K, Alawadhi H, Grimsditch M, Cardona M and Lauck R 2006 *Phys. Rev.* B **74** 165203
[40] Alawadhi H, Tsoi S, Lu X, Ramdas A K, Grimsditch M, Cardona M and Lauck R 2007 *Phys. Rev.* B **75** 205207
[41] Betzinger M, Friedrich C and Blügel S 2010 *Phys. Rev.* B **81** 195117
[42] Uddin J and Scuseria G E 2006 *Phys. Rev.* B **74** 245115
[43] Molepo M P and Joubert D P 2011 *Phys. Rev.* B **84** 94110
[44] Desgreniers S 1998 *Phys. Rev.* B **58** 14102
[45] Gómez-Abal R, Li X, Scheffler M and Ambrosch-Draxl C 2008 *Phys. Rev. Lett.* **101** 106404